Effects of Linking Topology on the Shear Response of Connected Ring Polymers: Catenanes and Bonded Rings Flow Differently

Reyhaneh A. Farimani[1,2] Zahra Ahmadian Dehaghani[3] Christos N. Likos[2] and Mohammad Reza Ejtehadi[1]

[1]*Department of Physics, Sharif University of Technology, Tehran, Iran*
[2]*Faculty of Physics, University of Vienna, Boltzmanngasse 5, 1090 Vienna, Austria*
[3]*International School for Advanced Studies (SISSA), Via Bonomea 265, 34136 Trieste, Italy*

We perform computer simulations of mechanically linked (poly[2]catenanes, PC) and chemically bonded (bonded rings, BR) pairs of self-avoiding ring polymers in steady shear. We find that BRs develop a novel motif, termed *gradient tumbling*, rotating around the gradient axis. For the PCs the rings are stretched and display another new pattern, termed *slip tumbling*. The dynamics of BRs is continuous and oscillatory, whereas that of PCs is intermittent between slip-tumbling attempts. Our findings demonstrate the interplay between topology and hydrodynamics in dilute solutions of connected polymers.

Polymer topology has profound and fascinating implications on the equilibrium and flow properties of polymer solutions and melts [1,2]. A prominent example of topologically constrained polymers are (unknotted) rings, which differ from their linear counterpart through the simple operation of joining the two ends together without any additional chemical modification or change in the solvent. Already this simple operation brings about spectacular changes in the properties of both the single molecule and concentrated solutions of the same. At the dilute limit, the condition of topology conservation leads to a scaling of the ring size with molecular weight following a self-avoiding exponent even for rings without excluded-volume interactions [3], and it introduces a concomitant topological potential between two rings [4]. In concentrated solutions and melts, the absence of free ends brings about once more dramatic changes in both the scaling of the ring sizes with molecular weight [5] and in their conformations, which are not any more akin to Gaussian random walks but feature fractal, treelike conformations [5,6]. Equilibrium dynamics is affected as well, resulting in power-law stress relaxation [7] and unique shear-thinning exponents [8], in addition to the occurrence of mutual ring-threading events. The latter results in the formation of reversible mechanical links that are responsible for viscosity thickening in extensional flow [9,10] and are believed to play a key role in the temperature-gradient vitrification in melts, resulting in the formation of an active topological glass [11]. In flow-driven dilute conditions, the combination of topology with hydrodynamic interactions brings about phenomena unique to ring polymers, such as vorticity swelling in shear, extensional, or mixed flows [12–15] as well as hydrodynamic inflation under steady shear [16]. The current interest in ring polymers is further enhanced by the biological relevance of circular DNA, which can be found naturally in the form of (supercoiled) bacterial plasmids [17], extrachromosomal DNA of eukaryotes [18], or in the kinetoplast DNA [19–21] of trypanosoma.

Going beyond simple cyclic macromolecules, mechanically interlocked [22–27] or chemically bonded rings [28,29] form a higher level of supramolecular, topological polymers. Advances in the synthesis of polycatenanes, macro-molecular structures made of concatenated ring polymers, have sparked interest in their study, revealing they exhibit distinct characteristics that differ significantly from those of traditional polymers due to their internal degrees of freedom. Dehaghanni *et al.* found that the gyration radius of polycatenane features two distinct power-law dependencies on ring size and the number of rings, as a consequence of the topological linking constraints [30]. In addition, novel types of intramolecular, topological entanglements present in these molecules have been recently discovered [31]. Chiarantoni *et al.* studied polycatenanes in channel confinement and found that, unlike regular polymers, they continue stretching in the strong confinement regime [32], whereas Chen *et al.* showed that polycatenanes have a linear response regime to very large forces, due to delayed force penetration in these structures [33]. Moreover, polycatenane solutions and melts also feature intriguing dynamics and phase behavior [34–36]. Additionally, polycatenanes are promising candidates for novel materials, such as mechanophores, molecular motors, and transmembrane ion channels [37–39]. In recent work, Soh *et al.* studied the kinetoplast under planar elongational flow, finding that the usual abrupt coil-stretch transition in linear polymers is absent for this concatenated network [40]. Otherwise, very little is known about the behavior of topologically linked, ring-based aggregates under nonequilibrium conditions and, in particular, under shear flow. Here we show that for the simplest case of two connected ring polymers, the type of linking (chemical bond vs mechanical
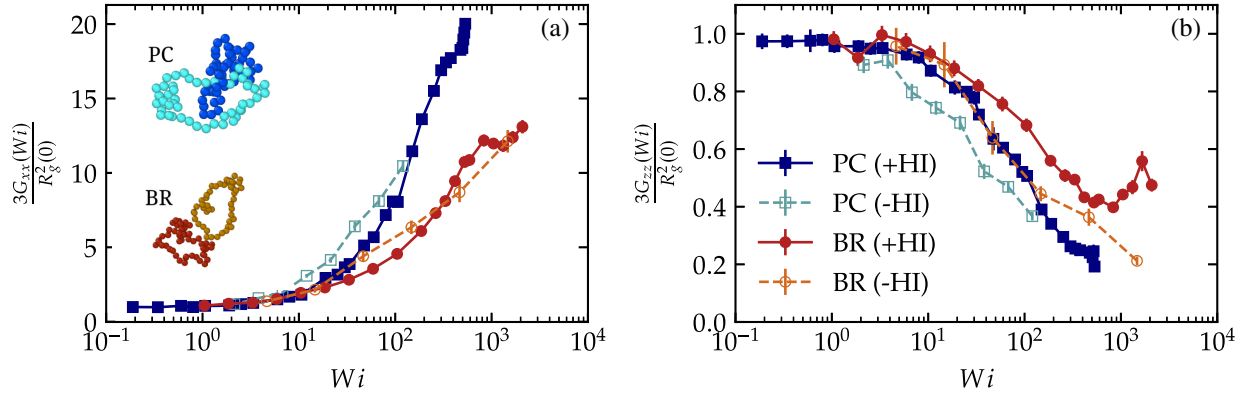
FIG. 1. Time averages of selected diagonal elements of the gyration tensor of the poly[2]catenane and the bonded rings system (entire molecules) in shear flow, as a function of the Weissenberg number, normalized over their equilibrium values, $R_g^2(0)/3$. (a) The flow-direction element, G_{xx}; (b) the vorticity direction element, G_{zz}. The dark blue-filled squares refer to PC (+HI), red-filled circles to BR (+HI), empty sky blue squares to PC (−HI), and empty orange circles to BR (−HI). The simulation snapshots in panel (a) show a PC molecule and a BR molecule at equilibrium ($Wi = 0$).

link) has profound consequences on the dynamical properties of the compound under steady shear and that novel dynamical patterns arise in these cases.

We consider two related supramolecular structures: a poly [2]catenane molecule (PC) consisting of two linked, self-avoiding ring polymers (Hopf link) and a system of two self-avoiding rings bonded by a bending- and torsion-free chemical bond (BR), see simulation snapshots in Fig. 1(a). Each ring contains $N = 50$ beads, connected to each other by fully flexible FENE bonds; details on the microscopic model and method are presented in the Supplemental Material [41]. We applied multiparticle collision dynamics (MPCD) as well as the random solvent variant of the same to simulate the dynamics, whereby the hydrodynamic interaction (HI) is included only in the former (denoted +HI) but not in the latter (denoted −HI) [50,51]. Steady shear is induced by employing Lees-Edwards boundary conditions [52], with $\hat{x}, \hat{y}, \hat{z}$ being the flow, gradient, and vorticity directions, respectively. We also use the molecule's longest relaxation time τ_R to define the dimensionless Weissenberg number $Wi = \tau_R\dot{\gamma}$. Details on the method and the relaxation time calculation can also be found in the Supplemental Material [41].

We have analyzed the conformations and dynamics of the compounds under steady shear at three different levels of description: for each ring component, for the entire macromolecule, as well as for an effective dimer consisting of the centers of mass of the two connected rings. Information on the shape and the dynamics of any polymer can be obtained from the gyration tensor, whose value at time t and for given Wi is defined as

$$G_{\alpha\beta}(t; Wi) = \frac{1}{\mathcal{N}} \sum_{i=1}^{\mathcal{N}} r_\alpha^{(i)}(t; Wi) r_\beta^{(i)}(t; Wi), \quad (1)$$

$\alpha, \beta \in \{x, y, z\}$, in which $\mathcal{N}$ refers to the number of monomers in the polymer, and it thus takes the value

$\mathcal{N} = N$ for an individual ring, $\mathcal{N} = 2N$ for the whole compound and $\mathcal{N} = 2$ for the effective dimer. Moreover, $r_\alpha^{(i)}(t; Wi)$ denotes the α Cartesian component of the position vector of monomer i in the polymer center of mass frame. The instantaneous gyration radius is expressed as $R_g(t; Wi) = (\text{Tr}[G(t, Wi)])^{1/2}$. We denote the eigenvalues of $G(t, Wi)$ with $\lambda_1(t; Wi) \geq \lambda_2(t; Wi) \geq \lambda_3(t; Wi)$ and $\hat{e}_i(t; Wi), i = 1, 2, 3$, represent the corresponding eigenvectors. Time averages are denoted $G_{\alpha\beta}(Wi) = \langle G_{\alpha\beta}(t; Wi)\rangle_t$ and $R_g(Wi) = \langle R_g(t; Wi)\rangle_t$; at equilibrium, $G_{\alpha\alpha}(Wi = 0) = R_g^2(Wi = 0)/3$. We consider here only the quantities $G_{xx}(Wi)$ and $G_{zz}(Wi)$; the results for $G_{yy}(Wi)$ are shown in the Supplemental Material Fig. S6 [41].

Figure 1(a) reveals that the PC stretches along the flow axis much stronger than the BR, illustrating that the topology is the most important factor in enhancing stretching, as the presence of HI does not markedly affect the amount of the stretch. Contrary to the entire state picture, the behavior of the individual rings comprising the PC and BR along the flow direction is practically indistinguishable, as shown in Fig. S4 [41].

The probability density function (PDF) of the instantaneous values of $G_{xx}(t; Wi)$, shown in Fig. 2, reveals dramatic differences between the PC and the BR. Whereas the expectation values for the PC are higher than those for the BR, the maximal stretching of the latter exceeds that of the former. At the same time, while the PDF for the PC shows a first-order-type transition from a state with a maximum at low values of $G_{xx}(t, Wi)$ at small Wi to a state with a maximum at high values of $G_{xx}(t, Wi)$ at large Wi, the maximum of the PDFs for the BR always remains at low $G_{xx}(t, Wi)$ values and the effect of increasing Wi is the stretching of the PDF to higher and higher $G_{xx}(t, Wi)$ values with a weak secondary maximum development at the highest Wi-value shown. This difference points to the
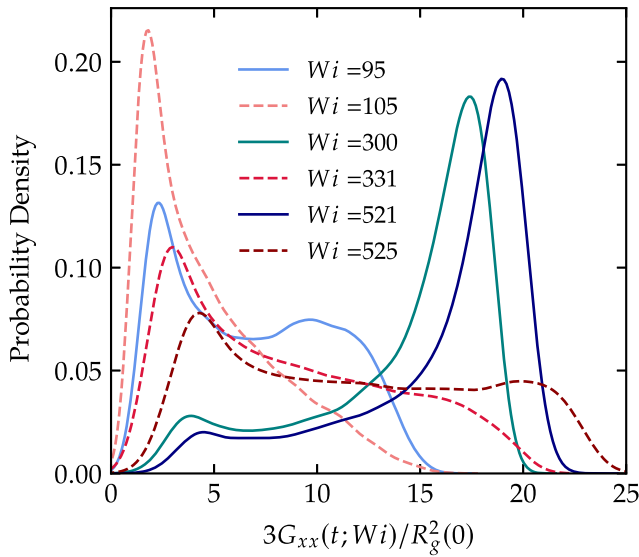
FIG. 2. Probability density function of $G_{xx}(t; Wi)$ normalized over $G_{xx}(0)$. Results are shown for PC (+HI), solid lines, and for BR (+HI), dashed lines, at various Weissenberg numbers, as indicated in the legend.

FIG. 3. Schematic of tumbling patterns. (a) Slip tumbling for PC (±HI). (b) Gradient tumbling for BR (+HI only).

presence of completely different dynamical motifs for the two molecules under shear.

It is known that vorticity swelling [13,15,16] takes place for individual rings under shear; we found that it also occurs for the constituent rings of the BR molecule in the +HI case but not for those of the PC, see Fig. S4 in the Supplemental Material [41]. Figure 1(b) demonstrates, in addition, the presence of vorticity swelling for the entire molecule, again only for the BR in the +HI case, whereas it is absent for the PC molecule regardless of the inclusion of HI, indicating a significant difference between the two molecules. This sets the stage for understanding a variety of dynamic features to follow. We further note that vorticity swelling is also seen in the dimer picture, as showcased in Supplemental Material [41] Fig. S5.

For the BR, the individual ring vorticity swelling, which is asynchronous for each ring due to thermal fluctuations, initiates solvent flow on the flow-vorticity plane, which disrupts the other ring. This makes the conformation of the BR orientationally unstable and sets a rotational pattern in motion in which the composite molecule rotates around an axis closely aligned to the gradient direction, extending thereby for a significant fraction of time into the vorticity direction. It is this extension that additionally contributes to the vorticity swelling of the *entire* bonded rings, seen in Fig. 1(b); a video and snapshots of this novel type of rotation can be found in the Supplemental Material [41]; see video 1. This is a tumbling motion, since the entire system rotates around its center of mass [53], but contrary to the usual tumbling that occurs around an axis roughly aligned with the vorticity direction, this rotational motion occurs around an axis approximately aligned with the
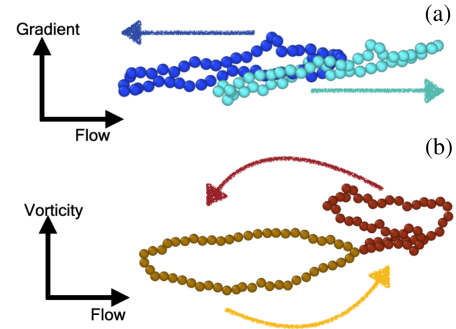
gradient axis. Accordingly, we coin the term gradient tumbling for this dominant dynamical motif of bonded rings under steady shear. The usual, vorticity tumbling, demonstrated in video 2 in the Supplemental Material [41], is also present in the case of bonded rings, but it is not the dominant dynamical pattern of motion. This is an incessant, continuous motion, as opposed to the intermittent dynamics featured by the PC.

The poly[2]catenane displays a very different dynamical pattern under shear, experiencing much fewer tumbling events than the bonded rings and featuring stable stretched conformations, which results in the appearance of the second maximum in the PDF of $G_{xx}(t; Wi)$ that dominates at high Wi values. The animation and snapshots from the trajectories show that the mechanical bond's freedom in the PC molecule plays a key role in allowing it to respond to the solvent-induced tension in a different fashion than the chemically bonded molecule. In video 3 in the Supplemental Material [41], it can be seen that in the PC, the two rings exchange their positions under shear in a way we term slip tumbling. Because of their particular connectivity in the form of a Hopf link, the two rings can undergo mutual slipping *through* each other while leaving their conformation tilted at a certain (low) angle with respect to the flow direction, and they are able to maintain this overall stretched configuration for longer intervals of time, whereas in topologies without mechanical links, when the polymer alignment is opposite of the flow field, the polymer starts to collapse and tumble [53]. Occasionally, such slip-tumbling events stay incomplete and the PC confirmation returns to the original one after such an unsuccessful attempt, see video 4 in the Supplemental Material [41]. Cartoons of the two types of tumbling are shown in Fig. 3.

Further evidence of the distinct response that the bonded rings and the poly[2]catenane have to shear is offered by the orientational correlations between the gyration eigenvectors in the two molecules. Indeed, vorticity swelling requires that each ring be oriented at an angle close to the flow direction, i.e., the eigenvectors $\hat{e}_{1,3}$ of vorticity-swollen rings lie almost parallel to the $\hat{x}$
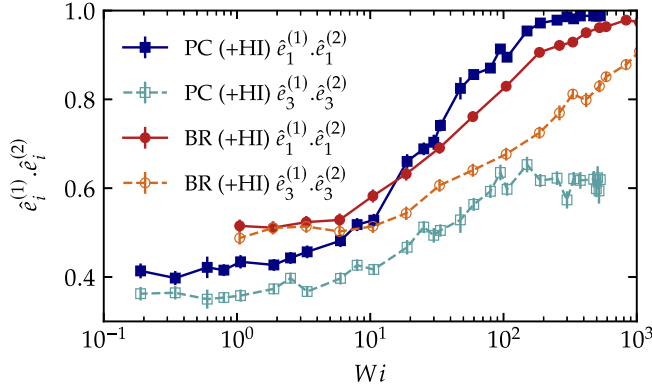
FIG. 4. Time averages $\hat{e}_i^{(1)} \cdot \hat{e}_i^{(2)}$ of the cosines between eigenvectors of the two rings in a PC or a BR. The case $i = 1$ corresponds to the largest eigenvalues and the case $i = 3$ to the smallest ones. The types of molecules and the $i = 1$, 3 are indicated by colors and symbols as shown in the legend.

FIG. 5. The relative x component (flow direction) of the rings's centers of mass as a function of time for $Wi \approx 500$. The red line corresponds to BR (+HI) at $\dot{\gamma} = 10^{-1.3}$ ($Wi = 525$) and the blue one to PC (+HI) at $\dot{\gamma} = 10^{-1.06}$ ($Wi = 521$).

and $\hat{y}$ directions, respectively. We consider, therefore, the time averages of the relative orientations of suitable eigenvectors, $\langle \hat{e}_i^{(1)}(t; Wi) \cdot \hat{e}_i^{(2)}(t; Wi) \rangle_t \equiv \hat{e}_i^{(1)} \cdot \hat{e}_i^{(2)}$, $i = 1$, 3, where the superscripts refer to rings (1) and (2) of the composite polymer; here, we have suppressed, for brevity, the dependence on the time-averaged quantity on Wi. Results in Fig. 4 show that the eigenvectors corresponding to the largest eigenvalue become increasingly aligned with growing Wi: starting from the value $\hat{e}_1^{(1)} \cdot \hat{e}_1^{(2)} \cong 0.5$, indicating a random orientation at equilibrium, all curves for both compounds and independently of the inclusion of HI approaches unity at $Wi \cong 10^3$, where the rings stretch along the flow direction. On the other hand, in Fig. 4 it can also be seen that the same does not hold true for the orientational correlation $\hat{e}_3^{(1)} \cdot \hat{e}_3^{(2)}$ between the eigenvectors that correspond to the lowest eigenvalue. For the BR rings, the curve is still monotonic, and it approaches unity at high Wi values, consistently with the fact that they feature vorticity swelling and thus they resemble discs oriented almost perpendicularly to the gradient direction. Although this joint orientation is possible for the case of rings connected by a chemical bond, the mechanical link in the case of the PC renders such an arrangement highly unlikely. As Wi grows, the mutual alignment of the "smallest" eigenvectors grows until it reaches a plateau value of about 0.6 at $Wi \approx 100$. The presence of a Hopf link imposes a local twist and, therefore, a strong local penalty for the two rings of a PC to attain disclike shapes, both oriented perpendicular to the y axis. Instead, they assume thin and mutually perpendicular orientations, which suppresses, therefore vorticity swelling giving rise instead to slip tumbling.

Strong evidence for the different types of dynamics featured by bonded rings and poly[2]catenanes is offered by looking at representations of typical trajectories, i.e., time series of certain characteristic quantities of the motion.
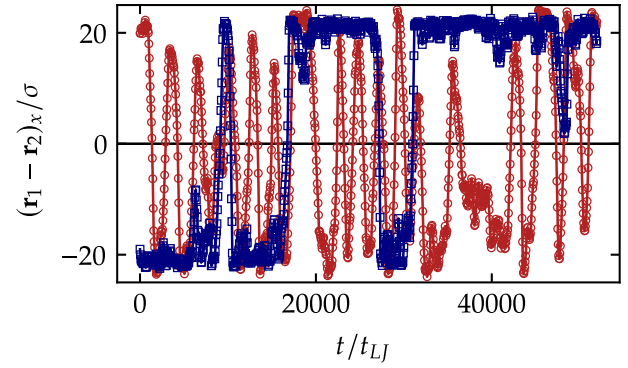
For this purpose, the effective dimer representation is the most suitable, as it employs a minimalistic description that captures nevertheless the salient properties of the system. First, we consider the x component of the relative separation $\mathbf{r}_1 - \mathbf{r}_2$ between the two poles of the dimer, shown as a time series for $Wi \cong 500$ in Fig. 5. The PC features two stable configurations with occasional flipping events caused by slip tumbling and thus it is characterized by intermittent dynamics, whereas the BR features incessant rotational motion characteristic of the dominant, gradient-tumbling pattern of the same. We have confirmed by simulation at selected points that our findings also remain valid for longer rings; see the Supplemental Material [41] Fig. S8.

We further consider the alignment angle $\theta(t; Wi)$ of the composite molecules with the flow axis by employing the instantaneous version of the time-average relation [54]:

$$\theta(t; Wi) = \frac{1}{2} \tan^{-1} \left[\frac{G_{xy}(t; Wi)}{G_{xx}(t; Wi) - G_{yy}(t; Wi)} \right]. \quad (2)$$

Results at $Wi \approx 500$ are presented in Fig. S7 in Supplemental Material [41]. The alignment angle of the PC is not only smaller in magnitude than that of the BR, but it features much less pronounced fluctuations as well affirming the property that the PC has much more stable orientation in space than the BR, a feature arising from its unique linking topology, allowing it to slip tumble and thus avoid turbulent tumbling events [53–55]. In addition, the angle is essentially always positive for both cases, indicating that vorticity tumbling is extremely rare. A quantitative analysis of the characteristic tumbling frequencies is presented in Supplemental Material [41] Fig. S9.

A reduced frequency of slip-tumbling events and suppressed shape fluctuations during slipping (PC), as opposed to incessant gradient and occasional vorticity tumbling (BR) explain the dramatic differences in the PDFs of the two, shown in Fig. 2. This observation is even more intriguing if compared to the results by Chen *et al.* [33],

who recently studied poly[n]catenane and bonded ring systems under extensional forces *in equilibrium*. It was found that the elastic modulus of poly[2]catenane is nearly double that of the bonded rings, i.e., for a given external force, the BR stretches more than the PC. In our case, for a given Wi, the BR can achieve longer maximum stretching compared to the PC, as seen in Fig. 2. However, the time average shows the opposite behavior due to tumbling events, a hydrodynamically induced pattern of motion absent when simply pulling the macromolecule by a bare force at both ends, as is the case in the work of Ref. [33].

We have carried out computer simulations of chemically bonded and mechanically linked ring polymers under shear with full consideration of the hydrodynamic interactions, establishing that connected polymer dynamics is very rich and strongly specific on the link type. These structures experience different pathways of tumbling unknown to other polymer topologies. Mechanically linked systems feature a stable stretched state and are independent of the presence or absence of hydrodynamic interactions and feature slip tumbling. Accordingly, we expect systems that possess a high number of mechanical bonds not to experience tumbling under shear flow, consistently with the observed behavior of kinetoplast under elongational flow [40]. While both chemically bonded and mechanically linked systems exhibit shear-thinning behavior, the latter maintain their stretched state for longer time intervals, resulting in a higher shear viscosity than their chemically bonded counterparts. On the other hand, chemically bonded ring pairs are highly agile under flow but, at odds with usual polymer dynamics, they display gradient-direction tumbling. Based on the fluctuating origin of this type of tumbling, we expect that bonding more and more rings chemically in a linear fashion would eventually suppress the emergence of such dynamics. Our results underline the intriguing interplay between topology, hydrodynamics, and thermal fluctuations in polymer solutions, and they are, in principle, experimentally observable in suitably constructed microfluidic devices [15,56].

[1] C. Micheletti, D. Marenduzzo, and E. Orlandini, Polymers with spatial or topological constraints: Theoretical and computational results, Phys. Rep. **504,** 1 (2011).

[2] M. Rubinstein and R. H. Colby, *Polymer Physics* (Oxford University Press, New York, 2003).

[3] J. M. Deutsch, Equilibrium size of large ring molecules, Phys. Rev. E **59,** R2539 (1999).

[4] M. D. Frank-Kamenetskii, A. V. Lukashin, and A. V. Vologodksii, Statistical mechanics and topology of polymer chains, Nature (London) **258,** 398 (1975).

[5] J. D. Halverson, W. B. Lee, G. S. Grest, A. Y. Grosberg, and K. Kremer, Molecular dynamics simulation study of non-concatenated ring polymers in a melt. I. Statics, J. Chem. Phys. **134,** 204904 (2011).

[6] A. Rosa and R. Everaers, Ring polymers in the melt state: The physics of crumpling, Phys. Rev. Lett. **112,** 118302 (2014).

[7] M. Kapnistos, M. Lang, D. Vlassopoulos, W. Pyckhout-Hintzen, D. Richter, D. Cho, T. Chang, and M. Rubinstein, Unexpected power-law stress relaxation of entangled ring polymers, Nat. Mater. **7,** 997 (2008).

[8] D. Parisi, S. Costanzo, Y. Jeong, J. Ahn, T. Chang, D. Vlassopoulos, J. D. Halverson, K. Kremer, T. Ge, M. Rubinstein, G. S. Grest, W. Srinin, and A. Y. Grosberg, Nonlinear shear rheology of entangled polymer rings, Macromolecules **54,** 2811 (2021).

[9] Q. Huang, J. Ahn, D. Parisi, T. Chang, O. Hassager, S. Panyukov, M. Rubinstein, and D. Vlassopoulos, Un-expected stretching of entangled ring macromolecules, Phys. Rev. Lett. **122,** 208001 (2019).

[10] T. C. O'Connor, T. Ge, M. Rubinstein, and G. S. Grest, Topological linking drives anomalous thickening of ring polymers in weak extensional flows, Phys. Rev. Lett. **124,** 027801 (2020).

[11] J. Smrek, I. Chubak, C. N. Likos, and K. Kremer, Active topological glass, Nat. Commun. **11,** 26 (2020).

[12] K. W. Hsiao, C. M. Schroeder, and C. E. Sing, Ring polymer dynamics are governed by a coupling between architecture and hydrodynamic interactions, Macromolecules **49,** 1961 (2016).

[13] M. Liebetreu, M. Ripoll, and C. N. Likos, Trefoil knot hydrodynamic delocalization on sheared ring polymers, ACS Macro Lett. **7,** 447 (2018).

[14] C. D. Young, J. R. Qian, M. Marvin, and C. E. Sing, Ring polymer dynamics and tumbling-stretch transitions in planar mixed flows, Phys. Rev. E **99,** 062502 (2019).

[15] M. Q. Tu, M. Lee, R. M. Robertson-Anderson, and C. M. Schroeder, Direct observation of ring polymer dynamics in the flow-gradient plane of shear flow, Macromolecules **53,** 9406 (2020).

[16] M. Liebetreu and C. N. Likos, Hydrodynamic in-flation of ring polymers under shear, Commun. Mater. **1,** 4 (2020).

[17] Front matter, in *Plasmid Biology*, edited by B. E. Funnell and G. J. Phillips (John Wiley & Sons, Ltd, New York, 2004).

[18] R. P. Koche *et al.*, Extrachromosomal circular DNA drives oncogenic genome remodeling in neuroblastoma, Nat. Genet. **52,** 29 (2020).

[19] A. R. Klotz, B. W. Soh, and P. S. Doyle, Equilibrium structure and deformation response of 2D kinetoplast sheets, Proc. Natl. Acad. Sci. U.S.A. **117,** 121 (2020).

[20] J. Chen, P. T. Englund, and N. R. Cozzarelli, Changes in network topology during the replication of kinetoplast DNA, EMBO J. **14**, 6339 (1995).

[21] P. He, A. J. Katan, L. Tubiana, C. Dekker, and D. Michieletto, Single-molecule structure and topology of kinetoplast DNA networks, Phys. Rev. X **13**, 021010 (2023).

[22] Q. Wu, P. M. Rauscher, X. Lang, R. J. Wojtecki, J. J. de Pablo, M. J. Hore, and S. J. Rowan, Poly [n] catenanes: Synthesis of molecular interlocked chains, Science **358**, 1434 (2017).

[23] S. Datta, Y. Kato, S. Higashiharaguchi, K. Aratsu, A. Isobe, T. Saito, D. D. Prabhu, Y. Kitamoto, M. J. Hollamby, A. J. Smith, R. Dagleish, N. Mahmoudi, L. Pesce, C. Perego, G. M. Pavan, and S. Yagai, Self-assembled poly-catenanes from supramolecular toroidal building blocks, Nature (London) **583**, 400 (2020).

[24] M. M. Tranquilli, B. W. Rawe, G. Liu, and S. J. Rowan, The effect of thread-like monomer structure on the synthesis of poly[n]catenanes from metallosupramolecular polymers, Chem. Sci. **14**, 2596 (2023).

[25] L. F. Hart, J. E. Hertzog, P. M. Rauscher, B. W. Rawe, M. M. Tranquilli, and S. J. Rowan, Material properties and applications of mechanically interlocked polymers, Nat. Rev. Mater. **6**, 508 (2021).

[26] G. Liu, P. M. Rauscher, B. W. Rawe, M. M. Tranquilli, and S. J. Rowan, Polycatenanes: Synthesis, characterization, and physical understanding, Chem. Soc. Rev. **51**, 4928 (2022).

[27] E. Orlandini and C. Micheletti, Topological and physical links in soft matter systems, J. Phys. Condens. Matter **34**, 013002 (2022).

[28] G. Polymeropoulos, G. Zapsas, K. Ntetsikas, P. Bilalis, Y. Gnanou, and N. Hadjichristidis, 50th anniversary perspective: Polymers with complex architectures, Macromolecules **50**, 1253 (2017).

[29] C. Chen and T. Weil, Cyclic polymers: Synthesis, characteristics, and emerging applications, Nanoscale Horiz. **7**, 1121 (2022).

[30] Z. Ahmadian Dehaghani, I. Chubak, C. N. Likos, and M. R. Ejtehadi, Effects of topological constraints on linked ring polymers in solvents of varying quality, Soft Matter **16**, 3029 (2020).

[31] Z. Ahmadian Dehaghani, P. Chiarantoni, and C. Micheletti, Topological entanglement of linear catenanes: Knots and threadings, ACS Macro Lett. **12**, 1231 (2023).

[32] P. Chiarantoni and C. Micheletti, Linear catenanes in channel confinement, Macromolecules **56**, 2736 (2023).

[33] Y.-X. Chen, X.-Q. Cai, and G.-J. Zhang, Topological catenation enhances elastic modulus of single linear polycatenane, Chinese Journal of Polymer Science **41**, 1486 (2023).

[34] P. M. Rauscher, K. S. Schweizer, S. J. Rowan, and J. J. de Pablo, Thermodynamics and structure of poly[n]catenane melts, Macromolecules **53**, 3390 (2020).

[35] P. M. Rauscher, K. S. Schweizer, S. J. Rowan, and J. J. de Pablo, Dynamics of poly[n] catenane melts, J. Chem. Phys. **152**, 214901 (2020).

[36] R. Staňo, C. N. Likos, and S. A. Egorov, Mixing linear chains with rings and catenanes: Bulk and interfacial behavior, Macromolecules **56**, 8168 (2023).

[37] M. Zhang and G. De Bo, A catenane as a mechanical protecting group, J. Am. Chem. Soc. **142**, 5029 (2020).

[38] E. R. Kay and D. A. Leigh, Beyond switches: Rotaxane-and catenane-based synthetic molecular motors, Pure Appl. Chem. **80**, 17 (2008).

[39] D. P. August, S. Borsley, S. L. Cockroft, F. della Sala, D. A. Leigh, and S. J. Webb, Transmembrane ion channels formed by a star of david [2] catenane and a molecular pentafoil knot, J. Am. Chem. Soc. **142**, 18859 (2020).

[40] B. W. Soh and P. S. Doyle, Deformation response of catenated DNA networks in a planar elongational field, ACS Macro Lett. **9**, 944 (2020).

[41] See Supplemental Material at http://link.aps.org/supplemental/10.1103/PhysRevLett.132.148101 for a description of the model, details on the calculations of polymer sizes, conformations, and dynamics, and videos of polymer motion patterns. The supplemental material includes in Refs. [42–49].

[42] L. Verlet, Computer experiments on classical fluids. I. Thermodynamical properties of Lennard-Jones molecules, Phys. Rev. **159**, 98 (1967).

[43] T. Ihle and D. M. Kroll, Stochastic rotation dynamics. I. Formalism, galilean invariance, and Green-Kubo relations, Phys. Rev. E **67**, 11 (2003).

[44] C. C. Huang, A. Chatterji, G. Sutmann, G. Gompper, and R. G. Winkler, Cell-level canonical sampling by velocity scaling for multiparticle collision dynamics simulations, J. Comput. Phys. **229**, 168 (2010).

[45] C. C. Huang, A. Varghese, G. Gompper, and R. G. Winkler, Thermostat for nonequilibrium multiparticle-collision-dynamics simulations, Phys. Rev. E **91**, 013310 (2015).

[46] M. Ripoll, K. Mussawisade, R. G. Winkler, and G. Gompper, Dynamic regimes of fluids simulated by multi-particle-collision dynamics, Phys. Rev. E **72**, 016701 (2005).

[47] S. Brown and G. Szamel, Structure and dynamics of ring polymers, J. Chem. Phys. **108**, 4705 (1998).

[48] P. M. Rauscher, S. J. Rowan, and J. J. de Pablo, Topological effects in isolated poly[n]catenanes: Molecular dynamics simulations and rouse mode analysis, ACS Macro Lett. **7**, 938 (2018).

[49] W. Chen, K. Zhang, L. Liu, J. Chen, Y. Li, and L. An, Conformation and dynamics of individual star in shear flow and comparison with linear and ring polymers, Macromolecules **50**, 1236 (2017).

[50] G. Gompper, T. Ihle, D. M. Kroll, and R. G. Winkler, Multi-particle collision dynamics: A particle-based mesoscale simulation approach to the hydrodynamics of complex fluids, in *Advanced Computer Simulation Approaches for Soft Matter Sciences III*, edited by C. Holm and K. Kremer (Springer Berlin Heidelberg, Berlin, Heidelberg, 2009), pp. 1–87.

[51] M. Ripoll, R. G. Winkler, and G. Gompper, Star polymers in shear flow, Phys. Rev. Lett. **96**, 188302 (2006).

[52] A. W. Lees and S. F. Edwards, The computer study of transport processes under extreme conditions, J. Phys. C **5**, 1921 (1972).

[53] P. G. de Gennes, Coil-stretch transition of dilute flexible polymers under ultrahigh velocity gradients, J. Chem. Phys. **60**, 5030 (1974).

[54] R. E. Teixeira, H. P. Babcock, E. S. G. Shaqfeh, and S. Chu, Shear thinning and tumbling dynamics of single polymers in the flow-gradient plane, Macromolecules **38**, 581 (2005).

[55] C. M. Schroeder, R. E. Teixeira, E. S. G. Shaqfeh, and S. Chu, Characteristic periodic motion of polymers in shear flow, Phys. Rev. Lett. **95**, 018301 (2005).

[56] M. Tanyeri and C. M. Schroeder, Manipulation and confinement of single particles using fluid flow, Nano Lett. **13**, 2357 (2013).